Solvent dynamics of aqueous halides before and after photoionization

Marco Reidelbach,[*,†,‡,¶] Michaela Schneeberger,[§,‡] Martin Sebastian Zöllner,[§,‡] Mei Bai,[‖,‡] Katharina Kubicek,[‡,⊥] Henning Kirchberg,[‖,‡,#] Christian Bressler,[⊥,‡] Michael Thorwart,[*,‖,‡] and Carmen Herrmann[*,§,‡]

†*Department of Chemistry, Universität Hamburg, Martin-Luther-King-Platz 6, 20146 Hamburg, Germany*

‡*The Hamburg Centre of Ultrafast Imaging, Hamburg, Germany*

¶*Now at: Zuse Institute Berlin, Takustraße 7, 14195 Berlin, Germany*

§*Department of Chemistry, Universität Hamburg,* Harbor *Bldg. 610, Luruper Chaussee 149, 22761 Hamburg, Germany*

‖*I. Institut für Theoretische Physik, Universität Hamburg, Notkestr. 9, 22607 Hamburg, Germany*

⊥*European XFEL, Holzkoppel 4, 22869 Schenefeld, Germany*

#*Now at: Department of Chemistry, University of Pennsylvania, Philadelphia, Pennsylvania 19014, USA*

E-mail: reidelbach@zib.de; michael.thorwart@physik.uni-hamburg.de; carmen.herrmann@chemie.uni-hamburg.de

Abstract

Electron transfer reactions can be strongly influenced by solvent dynamics. We study the photoionization of halides in water as a model system for such reactions. There are no internal nuclear degrees of freedom in the solute, allowing to uniquely identify the dynamics of the solvent. We simulate the equilibrium solvent dynamics for Cl^-, Br^-, I^- and their respective neutral atoms in water, comparing quantum mechanical/molecular mechanical (QM/MM) and classical molecular dynamics (MD) methods. On the basis of the obtained configurations, we calculate the extended X-Ray fine structure (EXAFS) spectra rigorously based on the MD snapshots and compare in detail with other theoretical and experimental results available in the literature. We find our EXAFS spectra based on QM/MM MD simulations in good agreement with their experimental counterparts for the ions. Classical MD simulations for the ions lead to EXAFS spectra that agree equally well with the experiment when it comes to the oscillatory period of the signal, even though they differ from the QM/MM radial distribution functions extracted from the MD. The amplitude is, however, considerably overestimated. This suggests that to judge the reliability of theoretical simulation methods or to elucidate fine details of the atomistic dynamics of the solvent based on EXAFS spectra, the amplitude and not only the oscillatory period need to be considered. If simulations fail qualitatively, as does the classical MD for the aqueous halogen atoms, the resulting EXAFS will also be strongly affected in both oscillatory period and amplitude. The good reliability of QM/MM-based EXAFS simulations, together with clear qualitative differences in the EXAFS spectra found between halides and their atomic counterparts, suggests that a combined theory and experimental EXAFS approach is suitable for elucidating the nonequilibrium solvent dynamics in the photoionization of halides, and possibly also for electron transfer reactions in more complex systems.

1 Introduction

Electron transfer is an important process in biology[1,2], catalysis[3–5], and artificial photosynthesis[6,7]. The environment (e.g., a solvent) plays an important active role in this process, rather than being a passive spectator[8–13], and recent advances with time-resolved techniques, including X-ray spectroscopy, have given new insight into how the nonequilibrium dynamics of the environment affects electron transfer[14–23]. For example, for transition metal complexes, solvation dynamics strongly modulate intramolecular electron transfer and localization, rather than just perturbing it[21].

The photodetachment of an electron from a solvated halide ion such as aqueous bromide, by ultraviolet or visible light,

$$\mathrm{Br}^-(\mathrm{aq}) \xrightarrow{\mathrm{h}\nu} \mathrm{Br}^\bullet(\mathrm{aq}),$$

represents an ideal model to study the elementary steps in nonequilibrium solvent dynamics in electron transfer: The lack of internal nuclear degrees of freedom of the halide ion allows us to focus on the pure influence of the solvent reorganization following internal electron rearrangement. Furthermore, the prompt transition from a hydrophilic (parent ion) to a hydrophobic (atomic radical) solute induces a substantial change of the caging solvent structure. Such an interplay between hydrophilic and hydrophobic interactions is also relevant for biological processes and for catalysis[24]. In addition, the dynamics of small inorganic radicals in solution are interesting in their own right for aerosol, marine, photo- and radiation chemistry studies[25]. Recent progress in ultrafast atomically resolving structural probes promises new insight and a more detailed picture of such guest–host interactions in disordered liquids under nonequilibrium conditions.

In the experiment, femtosecond time-resolution of pure laser-based methods in the visible to near-IR region has been achieved, and most notably transient absorption (TA) spectroscopy has been widely used to investigate the ultrafast dynamic response after photo-excitation of

aqueous halides[26–38]. However, the observation of pure solvation dynamics around the reactant with the TA method is challenging as it has high sensitivity towards changes in both electronic and vibronic energy levels, but is not directly sensitive to structural changes[39]. Such structural sensitivity is offered by X-rays. Solvation structures are inherently described in terms of radial distribution functions by experimental methods such as X-ray diffraction (XRD) and X-ray absorption spectroscopy (XAS)[40]. Specifically, the Extended X-ray Absorption Fine Structure (EXAFS)[28,38,39] is often a more appropriate probe for structural studies because of its intrinsic chemical specificity and short range sensitivity: This technique measures a less complex correlation function, as compared to X-ray diffraction, that contains accurate structural information on the first hydration shell structure[41].

Transient K- and L-edge EXAFS measurements for aqueous bromide and iodide at synchrotron X-ray sources, mostly with picosecond time-resolution, have been used to determine the local structure around the transient halide species emerging after optical laser-induced electron photodetachment[25,38,39,42]. Exploiting the $\chi(k)$ EXAFS signal, the oscillatory portion of the absorption coefficient, which is mainly sensitive to pair distribution functions[40], the water shell organization has been found to vary upon electronic structure changes. Specifically, some picoseconds after I^- photoexcitation, the solvent shell is dominated by hydrophobic interactions. This is drastically different from the intial hydrophilic situation in which long-term bonds are also formed between the I^- ion and water molecules[25,38], but a quantitative analysis of the solvent shell reorganization relies on a clear description of the solvation shell structure around the halide prior to laser excitation[41]. Moreover, further experimental investigations targeting the early nonequlibrium solvation dynamics after halide electron photodetachment using X-ray Free Electron Laser (XFEL) sources equally require a thorough understanding of the initial and "final" solvation structures, i.e., around the atomic halide and the atomic radical dominating $\sim 50\,\mathrm{ps}$ after halide electron photodetachment prior to the onset of the subsequent photochemistry[38].

The halide anion solvation[41–48,48–63,63–79] has been studied more intensively than that of their

analogeous halogen radicals[25,38,76,80], as the anions naturally occur in solution (prior to any modification such as, e.g., photoexcitation), and their solvation is a very important subject in itself as it governs, e.g., the Hofmeister series defining protein salting-in and salting-out[42]. Despite the intensive efforts to investigate the hydration properties of the anions, experimental and theoretical results by themselves reveal an inhomogeneous picture of the halide solvation shell structure[81]. From the theoretical side, these include density functional theory (DFT) and quantum mechanical/molecular mechanical (QM/MM) simulations[43–45,48,63,66,71], Car–Parrinello molecular dynamics (MD) simulations[41,45,46,75,76,78], classical MD simulations[41,47–49,67,77], MD simulations involving data-driven potential energy functions[82,83], and Monte Carlo simulations[50]. Experimentally, the hydration properties have been studied using neutron and X-ray diffraction[51,52], X-ray absorption spectroscopy[25,38,42,44,53–60], and Raman and Infrared (IR) spectroscopies[61,84,85]. While mostly the solvating water molecules were found oriented so as to each produce a single HO–H$\cdots$X$^-$ hydrogen bond (X = Cl$^-$, Br$^-$, and I$^-$)[42], the studies report significantly scattered first-shell X–O distances and coordination numbers: 2.70 to 3.30 Å and 4.0 to 8.9 for chloride, 3.19 to 3.40 Å and 4.2 to 8.9 for bromide, and 3.02 to 3.70 Å and 4.2 to 10.3 for iodide[41,49,86]. On the one hand, the deviating results underline the difficulty of defining the halide coordination shells due to their diffuse character, and due to the fast water exchange between the first and second hydration shells (residence time is on the order of picoseconds[81,86]). On the other hand, while the EXAFS structural approach is very powerful as discussed above, at room temperature it has an estimation accuracy of ±25 % in coordination number and ±0.03 Å in bond length[42,87,88]. Overall, this leads to a considerable uncertainty in the detailed atomistic solvent structure and dynamics around halide ions and their radical atoms.

The challenges just described highlight the importance of complementing experimental studies with theoretical investigations for gaining insight and understanding[89,90]. In particular, MD simulations allow for sampling the phase space accessible to the system of interest under given thermodynamic conditions. An ensemble of microscopic configurations is retrieved, from which

one can compute any structural ensemble-averaged observable, such as the EXAFS signal[91]. This allows us to determine synthetic EXAFS spectra in which the effects of the disorder (i.e. the heterogeneity of the environments) are intrinsically taken into account[91]. Thus, the comparison of computed and experimental EXAFS spectra constitutes a much more robust way to analyse data than unconstrained peak fitting approaches[91]. Accordingly, in this work we present and analyze QM/MM as well as classical MD simulations and the resulting EXAFS spectra, and compare them with experimental EXAFS data from the literature.

Many quantum chemical simulations have been performed for cluster models of water molecules around the halides[53,92,93]. However, only few simulations have been compared with experimental observables[41]. D'Angelo et al. have performed a K-edge EXAFS study of bromide ions in aqueous solution using classical MD simulations.[54], an approach which was subsequently extended into the supercritical regime of water by Wallen et al. [94]. The derived Br-O radial distribution function was used with the integral formulation of the EXAFS equation to simulate the EXAFS theoretical signal. This was found to be in very good agreement with the experimental data. In later studies, D'Angelo et al. used a complimentary approach and examined the hydration properties of the bromide aqua ion using state-of-the-art DFT-based molecular dynamics methods with dispersion-corrected atom-centered pseudopotentials for water, comparing with classical molecular dynamics simulations[41]. A comparison with EXAFS experimental data showed a good (poor) agreement between the DFT simulation (classical simulation) and the EXAFS experimental signal. The authors concluded that the main reason for the poor performance of the classical simulation was the neglect of polarization effects in the classical ion–water interaction potentials[41]. Recently, Migliorati et al.[81] have investigated the hydration properties of halide aqua ions by combining classical MD structural results with EXAFS experimental data and checked the capability of three halide–water interaction potentials to properly describe the structural properties of halide aqueous solutions, obtaining a very good agreement for one particular parameter set[81]. A more comprehensive comparison between EXAFS spectra reconstructed from the radial distribution functions obtained from

different theorectial approaches — classical, QM/MM and full quantum (DFT) molecular dynamics simulations — and experimentally measured EXAFS spectra has been performed for the L_3 X-ray absorption edge of aqueous iodide by Pham et al.[45]. QM/MM simulations delivered a satisfactory description of the EXAFS signal, while nonpolarizable classical simulations were somewhat less satisfactory and DFT-based simulations performed poorly[45]. Data-driven many-body models have equally lead to very good agreement with experimental EXAFS data for aqueous halides[82,83].

Here, we expand on these studies by calculating directly EXAFS spectra using the molecular configurations obtained from the QM/MM and/or MD simlutations for the halide anions I^-, Br^- and Cl^- and for their atomic-radical counterparts I^0, Br^0 and Cl^0 in aqueous solution. No information other than nuclear coordinates of the solute and solvent molecules enter in the calculation of the EXAFS spectra. In particular, no adjustable parameters such as k-dependent phase shifts, Debye–Waller factors, or effective Coulomb parameters are used. This allows for a comprehensive comparison in which all the different systems, before (anionic) and after (atomic) photoionization, are described with the same theoretical methodology.

We compare with experimental EXAFS spectra for the ions from the literature[42] to understand the reliability of the QM/MM and/or MD simulations. The Fourier transform of the EXAFS signal back to real space allows us to extract quantitative spatial information. Moreover, we examine how strongly the EXAFS spectra depend on the different numerical methods applied, or, in other words, how sensitive the EXAFS signal is to the respective simulation parameters and thus how reliable EXAFS is as an indicator for the reliability of the QM/MM and MD simulations. We analyze the solvation shells and determine how ionization, i.e., a change from the anionic halide to the atomic radical, and property changes, e.g. van-der-Waals radii, polarizability etc., within the homologue halide series (Cl, Br, I) affect the radial distribution functions (RDFs), in particular their peak locations, as well as the structure of the EXAFS peaks. Also, we present a comparative overview of RDF maxima and minima from previous simulations and experiments from the literature. In general, our results, which are based on

microscopic numerical simulations, confirm the previously known solute–solvent structures obtained by fitting. The QM/MM-derived EXAFS spectra of the ionic halides in water are in very good agreement with measured ones. When compared to the EXAFS data on the basis of configurations from classical MD simulations, we notice good agreement with respect to the oscillatory period and the decay, but find deviations in the absolute signal magnitude. For the neutral atoms, the classical and QM/MM-derived EXAFS spectra deviate strongly from each other both with respect to oscillatory amplitude and period. This indicates that QM/MM simulations (or similar quality) are required to obtain reliable molecular configurations and thus reliable EXAFS spectra when studying the photoionization of aqueous halides. Our results provide crucial input for further theoretical and experimental investigations, in particular for studies of the nonequilibrium dynamics on ultrafast time scales following electron photodetachment of the halide anions.

2 Methods

We have performed molecular dynamics simulations of chloride (Cl^-), bromide (Br^-), iodide (I^-) ions and their neutral atom configurations (Cl^0, Br^0, and I^0) in water using the simulation package CP2K 7.1[95]. All simulations were carried out in the canonical ensemble (NVT) with a single halide ion/halogen atom solvated in a cubic box ($18.19^3\,\text{Å}^3$) under periodic boundary conditions, containing 199 water molecules at 298 K. The temperature was controlled with an adaptive Langevin thermostat[96] (Langevin / Nosé–Hoover time constants detailed below). Positions and momenta of all atoms were propagated in time by the velocity Verlet algorithm[97] with a time step of 0.5 fs.

For the QM/MM simulations, to ensure a proper description of the solute–solvent interactions, the halide ions/halogen atoms and their first solvent shell were treated quantum mechanically, following the Born–Oppenheimer MD scheme, using the Becke-Lee-Yang-Parr (BLYP) func-

tional[98,99] with Grimme's dispersion (D3) corrections[100], molecularly optimized double-zeta valence polarized basis sets[101] (DZVP-MOLOPT), Goedecker–Teter–Hutter (GTH) pseudopotentials[102–104] for the core electrons, and a density cutoff of 280 Ry. More distant water molecules were treated with molecular-mechanics (MM) using the TIP3P model[105] as originally implemented in CHARMM[106]. Both regions were coupled electrostatically. While the halide ions/halogen atoms were restricted to the center of the spherical QM subsystem, the assignments to the QM or MM regions for the water molecules were evaluated in each simulation step. Only water molecules within a certain radius (4.5 Å for Cl^-/Cl^0 and Br^-/Br^0, 5.0 Å for I^-/I^0) were assigned to the QM subsystem. Fictitious effects at the QM/MM boundary were reduced by introducing a buffer region, surrounding the QM subsystem, with a radius of 3.0 Å, two consecutive force evaluations per simulation step, and an abrupt force-mixing scheme. The buffer region was used in a first force evaluation to extend the QM subsystem to obtain more accurate forces acting on the actual QM atoms. Likewise, the QM subsystem was reduced in a second force evaluation to the halide ions/halogen atoms to assign more accurate forces acting on the actual MM atoms. The adaptive buffered (AdBuff) QM/MM simulation scheme was used within the framework of this study as implemented in CP2K[107].

For comparison with the QM/MM approach, purely classical MD simulations were performed using the CHARMM force field parameters. The water moelcules weere treated with the same original TIP3P model as in the MM part of our QM/MM simulations.

The solvated systems were built with PACKMOL 18.169[108]. Following two 10 ps equilibration runs with strong and weak thermostat time constants of 10/10 fs or 100/100 fs, respectively, a 20 ps preparatory run was performed to generate five structurally independent starting configurations picked after 4, 8, 12, 16, and 20 ps. To speed up the preparatory phase, the buffer region was turned off. Subsequently, a 25 ps AdBuff QM/MM run (5 ps equilibration + 20 ps production) was performed per starting configuration, with thermostat time constants of 370/75 fs. Thereby, 100 ps of AdBuff QM/MM simulation data were obtained per setup to characterize the solute–solvent interactions in equilibrium.

For the classical simulation, three 25 ps runs (5 ps equilibration + 20 ps production) were performed for each atom species. Therefore 75 ps of classical MD simulation data were obtained per setup.

The AdBuff QM/MM simulations were visualized with VMD[62] and analyzed with our own PYTHON scripts.

EXAFS spectra were calculated using the FEFF8 software package[109]. As input data, we use the coordinates of each atom (H, O, and the absorbing atom) obtained from the MD simulations. In addition, we specify the nature of the absorbing edge of the solute (K-edge or L1-edge) in the input data of FEFF8. Moreover, we point out that FEFF8 has the option to specify Debye-Waller factors which describe vibrations of lattice atoms in solid state materials. In our case of a solvent host, we simulate the solvent molecules and their dynamics explicitly and use all of their configurations as input for FEFF8, such that the Debye-Waller factors are irrelevant and thus are all set to 1. The EXAFS spectrum of each individual MD snapshot is then calculated separately, and the resulting collection of more than 2000 EXAFS spectra is averaged over all snapshots. For a direct comparison with experimental EXAFS spectra, we apply a shift in energy whose precise value is taken as a fitting parameter (see more detailed discussion below). Furthermore, the Fourier transform of the EXAFS signal back to real space is calculated numerically to obtain spatial information about the relative positions of the solute and the atoms of the solvent molecules.

3 Molecular Dynamics Simulations

We have performed equilibrium AdBuff QM/MM simulations of Cl^-, Br^-, I^- ions, and their neutral, atom configurations (Cl^0, Br^0, and I^0) in water to gain further insights into individual solute–solvent configurations and to confirm the applicability of our simulation setup. For this purpose, we have compared several structural and dynamical parameters emerging from our

simulations with previous experimental and theoretical studies.

3.1 Radial distribution functions from QM/MM simulations

The radial distribution function (RDF), $g(r)$, is ubiquitously used to characterize the solvation shell of particles. In principle, it provides the probability of finding a particle at a distance r from a reference particle and is defined as

$$g(r) = \frac{\langle n(r) \rangle}{4\pi r^2 \delta r \rho_0}, \tag{1}$$

where $\langle n(r) \rangle$ is the average number of particles in the volume slice $4\pi r^2 \delta r$ and ρ_0 is the particle's bulk density. In Figure 1, average RDFs are depicted for all QM/MM simulation setups (top) and for the purely classical MD setups (bottom). The relevant properties of the RDFs are summarized and compared with the literature in Table 1.

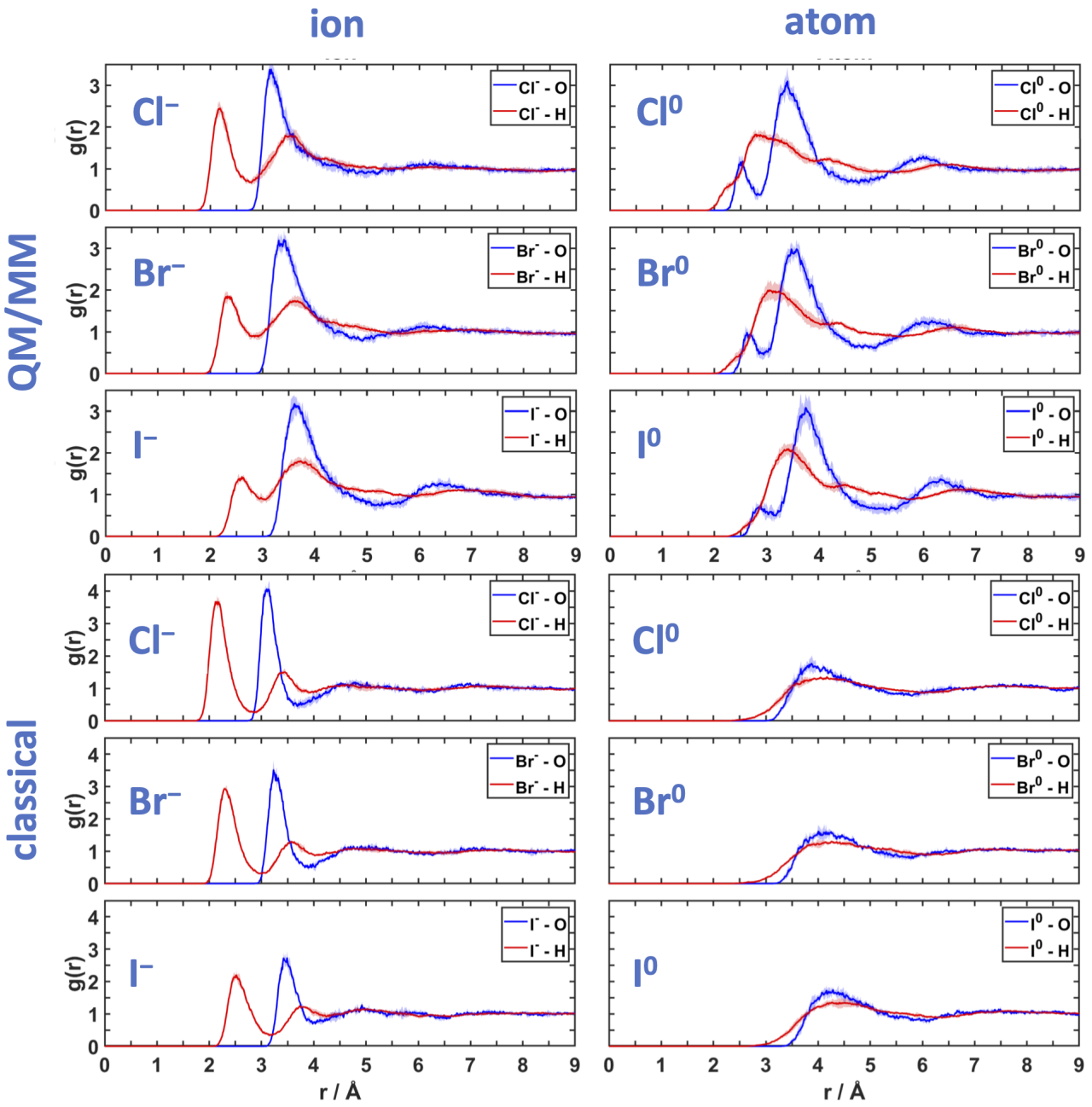

Figure 1: Oxygen (blue) and hydrogen (red) RDFs for the ion (left) and atom (right) configuration of Cl (top), Br (middle), and I (bottom) in water. RDFs were calculated from 20ps of ADBuff QM/MM (top) or classical MD (bottom) simulation as described in Sec. 2. Confidence intervals Δx, indicated in light blue and red, were calculated as $\Delta x = s(\bar{x})t(\alpha = 0.05, n-1)$, where $t(\alpha = 0.05, n-1)$ is the quantile of Student's t distribution with significance level α and n samples, and $s(\bar{x})$ is the standard error.

Table 1: Position (in Å) of the RDF maxima (+) and minima (−) from Figure 1 and selected previous studies. Values were obtained experimentally by empirical potential structure refinement from neutron diffraction (ND) or theoretically by classical (MM), quantum (QM), and mixed (QM/MM) calculations. Standard deviations of the individual runs are given in parentheses. MC refers to the Monte Carlo simulations employed in Ref.[25].

Cl^-					Cl^0						
O_+^1	H_+^1	O_-^1	type	ref	O_+^1	O_+^2	H_+^1	O_-^1	O_-^2	type	ref
3.17	2.19	5.21	QM/MM	our	2.54	3.50	2.80	2.81	4.78	QM/MM	our
(0.02)	(0.02)	(0.28)	QM/MM	our	(0.03)	(0.05)	(0.07)	(0.04)	(0.13)	QM/MM	our
3.10	2.15	3.68	MM	our	3.87	-	4.17	5.79	-	MM	our
(0.06)	(0.20)	(0.08)	MM	our	(0.22)	-	(0.04)	(0.02)	-	MM	our
3.14	2.17	3.77	ND	[52]	2.70	-	-	-	-	QM	[80]
3.14	2.21	3.78	QM	[63]							
3.24	2.42	4.00	QM/MM	[43]							
3.24	-	3.63	QM/MM	[44]							
3.23	-	4.05	MM	[110]							
3.36	2.37	3.75	MM	[111]							
Br^-					Br^0						
O_+^1	H_+^1	O_-^1	type	ref	O_+^1	O_+^2	H_+^1	O_-^1	O_-^2	type	ref
3.41	2.33	4.91	QM/MM	our	2.62	3.57	3.05	2.94	5.08	QM/MM	our
(0.05)	(0.03)	(0.28)	QM/MM	our	(0.05)	(0.07)	(0.15)	(0.08)	(0.20)	QM/MM	our
3.23	2.29	3.90	MM	our	4.01	-	4.26	5.82	-	MM	our
(0.30)	(0.05)	(0.07)	MM	our	(0.18)	-	(0.02)	(0.04)	-	MM	our
3.35	2.38	3.96	ND	[52]	3.00	3.70	-	-	-	MM(MC)	[25]
3.33	2.38	3.94	QM	[112]	2.80	-	-	-	-	QM	[80]
3.41	2.49	4.13	QM/MM	[64]							
3.33	-	4.04	QM/MM	[65]							
3.42	-	4.30	MM	[110]							
3.32	2.39	-	MM	[64]							
I^-					I^0						
O_+^1	H_+^1	O_-^1	type	ref	O_+^1	O_+^2	H_+^1	O_-^1	O_-^2	type	ref
3.62	2.61	5.15	QM/MM	our	2.89	3.75	3.42	3.18	5.35	QM/MM	our
(0.05)	(0.05)	(0.23)	QM/MM	our	(0.06)	(0.06)	(0.06)	(0.08)	(0.22)	QM/MM	our
3.49	2.52	3.98	MM	our	4.29	-	4.27	6.07	-	MM	our
(0.20)	(0.15)	(0.03)	MM	our	(0.10)	-	(0.10)	(0.06)	-	MM	our
3.62	2.65	4.31	ND	[52]	-	3.80	3.60	-	5.48	QM/MM	[38]
3.60	2.64	4.33	QM	[45]	2.80	-	-	-	-	QM/MM	[38]
3.75	2.78	5.19	QM/MM	[113]	2.90	4.00	3.55	3.20	-	QM	[76]
3.47	2.62	5.22	QM/MM	[45]							
3.64	-	4.50	MM	[110]							
3.55	2.55	-	MM	[77]							

3.1.1 Solvated anions

The QM/MM RDFs of Cl^-, Br^-, and I^- display similar features, i.e., a hydrogen peak is followed by an oxygen peak and a second hydrogen peak. While the individual peak positions increase with increasing van der Waals radius from Cl^- to Br^- to I^-, a separation of roughly 1 Å (or a covalent O-H bond) is maintained for the first hydrogen and oxygen peaks. Thus, a hydrophilic solvation picture emerges, in which the closest water molecules point with one of their hydrogen atoms directly towards the ion. The second hydrogen peak stems from the hydrogen atoms which are not oriented towards the ion. They are more flexible, resulting in broader peaks. They are most likely responsible for the hydrogen bonding within the solvent shells. Despite the overall similarities, the individual RDFs vary in detail. First of all, the minimum separating the first two hydrogen peaks becomes less pronounced with increasing ion size, indicating a stronger intermixing and thus a more flexible solvent shell for larger ions. Decreasing water residence times in the solvent shell, evaluated following the approach by Hofer et al[114], (3.28, 2.10, and 2.05 ps for Cl^-, Br^-, and I^-, respectively) further support this. In addition to the increased flexibility, a second oxygen peak, most likely related to the second solvent shell, emerges for larger ions.

Numerous experimental and theoretical investigations have focused on the RDFs of Cl^-, Br^-, and I^- in water. To determine the accuracy of our RDFs, we compared them with RDFs from neutron diffraction experiments, since these experiments are able to resolve oxygen and hydrogen peaks. We also compare with previous studies employing related simulation setups, i.e., QM/MM or full QM simulations. Overall, the positions of the first oxygen and hydrogen peaks agree quite well with experiments (maximal deviation of 0.06 Å) and the full QM simulations (maximal deviation of 0.08 Å). In addition, the RDFs show, in most cases, less pronounced deviations from these reference values than previous QM/MM simulations. A critical aspect of our RDFs is the position of the first oxygen minimum, which is substantially shifted to larger distances compared to experiments as well as to full QM simulations. This may be at least

partially related to the minimum being very shallow in our simulations, in particular for the smaller anions, with a resulting large uncertainty of its detailed value. While previous QM/MM studies of Cl^- and Br^- led, in most cases, only to marginal shifts of the first oxygen minimum compared to the references, the deviation for I^- is substantial and comparable to our results. Interestingly, Pham et al[45] found EXAFS spectra, calculated from their I^- QM/MM simulations, in good agreement with experiments despite the substantial shift of the first oxygen minimum. Hence, we believe that our AdBuff QM/MM simulations will accurately capture EXAFS experiments of solvated halide ions.

We further compare our results from QM/MM simulations with purely classical MD simulations, obtained with otherwise the same settings. The classical first oxygen and hydrogen peaks are shifted to smaller distances compared to the QM/MM RDFs. Br^- shows the largest oxygen shift of -0.18Å, followed by I^- with -0.13Å while the shift for Cl^- is small (-0.07Å). The hydrogen peaks are shifted less compared to the oxygen peaks (-0.04Å for Cl^- and Br^-, and -0.08Å for I^-). The first oxygen minimum is shifted strongly to smaller distances: -1.53Å Cl^-, -1.01Å Br^-, and -1.17Å I^-, putting them considerably closer to the experimental and QM reference values. Even though this might suggest that we should proceed with classical rather than QM/MM simulations, it should be kept in mind that classical force fields will have problems describing the radical nature of the photoionized atoms. Fully QM simulations are, on the other hand, much more expensive than the QM/MM ones we are analyzing here. Overall, the oxygen peaks appear much sharper, and accordingly, the minima between the first and second peaks become more pronounced. This suggests that the first solvation shell appears much less flexible when describing the systems by purely classical force fields.

In contrast with the oxygen minima, the deviations of our classical peak positions compared to the experiment (maximal deviation of 0.13Å) and fully QM simulation (maximum deviation of 0.12Å) are larger than the deviations of our QM/MM simulations from these reference values. There are, however, classical simulations reported in the literature with smaller deviations, indicating that with the right classical setup RDFs of halogen ions could be calculated more

accurately yet less expensively by omitting the QM part. Nontheless, as we are interested in the transition from ion to atom case, we need a suitable setup that can accurately simulate both. In the following chapter we will discuss and compare the results of QM/MM and classical simulation for the atom case and show why purely classical simulations are not suitable for studying the solvent dynamics after ionization.

3.1.2 Solvated neutral atoms

The RDFs of Cl^0, Br^0, and I^0 differ substantially from their charged counterparts. Here, a small oxygen peak is followed by a broad hydrogen peak and a second, larger oxygen peak. Once again, the individual peak positions follow the size of the solvated halogen atom, but the clear, atom-independent separation of the first hydrogen and oxygen peaks is lost. Instead, the hydrogen peak is 0.26, 0.33, and 0.53 Å more distant than the first oxygen peak, and 0.70, 0.52, and 0.33 Å closer than the second oxygen peak of Cl^0, Br^0, and I^0, respectively. Consequently, the hydrophilic solvation picture, in which the closest water molecules point with one of their hydrogen atoms directly towards the solute, is lost.

Solvated Cl^0, Br^0, and I^0 have received less attention in the literature than their ionic counterparts. Still, a consistent picture has emerged in which the water molecules form a more distant cage around the solvated halogen atoms corresponding to the prominent (second) oxygen peak in our RDFs. When comparing the position of the prominent oxygen peak from solvated I^- (neutron diffraction[52]) and I^0 (our AdBuff QM/MM simulations and those by Pham et al[38]), a shift of roughly 0.15 Å could be observed, while QM and MM simulations of I^0 and Br^0, respectively, suggest a shift of roughly 0.35 Å compared to experiments of the corresponding ion. In addition to the more distant solvent cage, transient complexes formed by the halogen atom and a single water molecule had been observed. In our setup, these complexes are stable throughout the simulations, indicated in the RDFs by the small (first) oxygen peaks. For I^0, the small oxygen peaks of other QM/MM and QM simulations are reproduced well, while theoreti-

cal calculations of Cl^0/Br^0 – water complexes, missing the environment, and MM simulations of Br^0 suggest somewhat larger distances. Previous investigations suggest an increasing complex stability with increasing electron affinity, i.e., the complex stability increases from I^0 to Br^0 to Cl^0 [38,80]. Our QM/MM simulations confirm this trend, when comparing the height of the first oxygen minimum, indicating, once again, more intermixing between the peaks with increasing atom size and thereby less complex stability with decreasing electron affinity. This is further supported by a decreasing well depth on the free energy surface (0.59, 0.53, 0.38 meV for Cl^0, Br^0, and I^0, respectively) with increasing atom size as suggested before [38]. Hence, we believe that our adaptive buffered QM/MM simulations would accurately capture EXAFS experiments of solvated halogen atoms.

3.2 Radial distribution functions from classical MD simulations

We also simulated the atom species using purely classical MD simulations, with drastically different results. There is no small first peak which would indicate the formation of a complex of the atom and a water molecule, in contrast to the QM/MM case. This can be attributed to the lack of proper parameters for radical–water binding in the force field, and might be remedied by going to reactive force fields (and by putting the effort into their proper parametrization). The only oxygen peak in the atom case (corresponding to the second oxygen peak in the QM/MM simulations) is shifted to larger distances (between +0.37Å and +0.54Å) and much less pronounced than in the QM/MM simulations. The hydrogen peaks are shifted even more (between +1.37Å and +0.85Å), such that they almost overlap with the oxygen ones. Consistent with the QM/MM simulations, there is no sign of hydrophilic behaviour. Nonetheless, due to not showing complex formation and due to the large qualitative deviations in the RDFs, the pure MM simulations fail at simulating the atom case.

3.3 Solvent shell characterization

To further substantiate the validity of our AdBuff QM/MM simulations, we determined additional parameters characterizing the aqueous solvation of halide ions and halogen atoms and compare them with the literature. Integration of the first peak of the hydrogen and oxygen RDFs provides the number of hydrogen and oxygen atoms coordinated within the first solvent shell. Neutron diffraction experiments[52] suggest 6.4, 5.9, and 5.8 coordinated hydrogen atoms and 7.1, 6.7, and 6.7 coordinated oxygen atoms for Cl^-, Br^-, and I^-, respectively. Similar coordination numbers, at least for the oxygen atoms, were obtained by isotope substitution[86,115] (Cl^-) and EXAFS[54,94] (Br^-), while X-ray diffraction experiments[86] (I^-) yielded a broader range (4.2 - 9.6). With our AdBuff QM/MM simulations, we obtained slightly lower numbers of coordinated hydrogen atoms (5.5, 5.4, and 4.7 for Cl^-, Br^-, and I^-), while the number of coordinated oxygen atoms (21.6, 18.6, and 21.5 for Cl^-, Br^-, and I^-), is overestimated substantially due to the aforementioned shift of the minimum in the oxygen RDFs.

For Cl^0, Br^0, and I^0, on the other hand, the AdBuff QM/MM simulations suggest 1.0, 1.0, and 1.1 or 16.3, 18.8, and 21.6 coordinated oxygen atoms within the first and second oxygen peak, respectively, while 49.5, 51.3, and 56.2 coordinated hydrogen atoms are suggested for the first hydrogen peak. Previously, Pham et al[38] determined 20 – 25 coordinated oxygen and 50 – 60 coordinated hydrogen atoms in the more distant solvent shell of I^0, corresponding to our second oxygen and first hydrogen peak, which agrees quite well with our results. No such data is available for Cl^0 and Br^0.

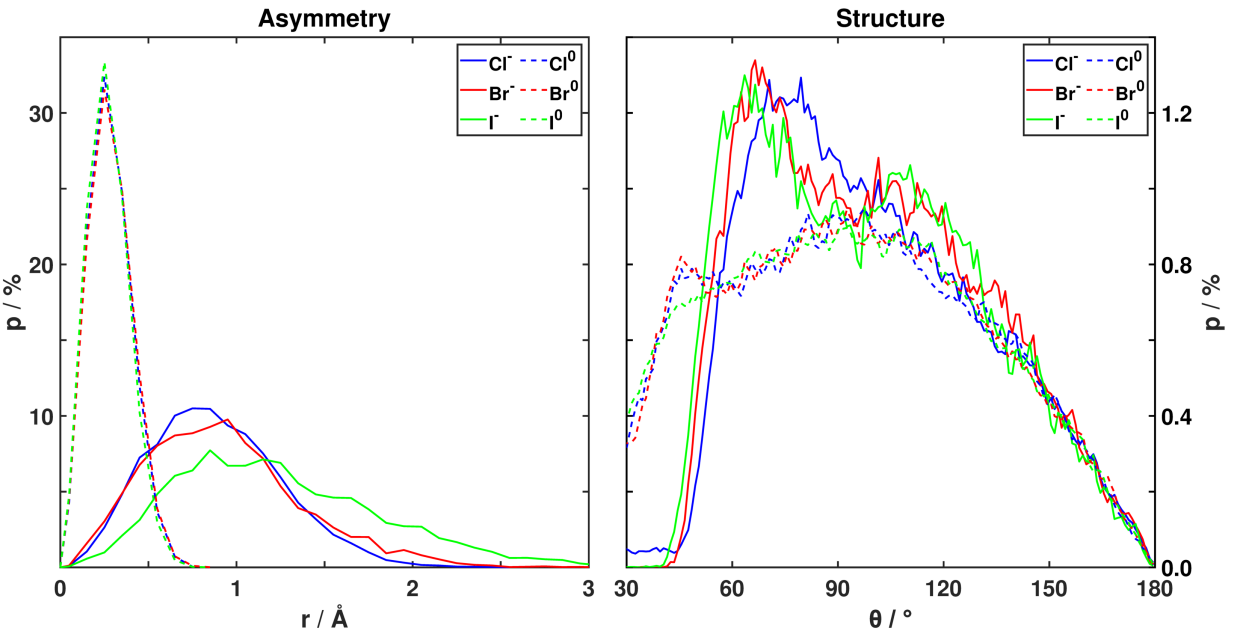

Figure 2: Probability distribution describing the asymmetry (left) and structure (right) of the first solvation shell of Cl (blue), Br (red), and I (green) in the ion (solid lines) and atom (dashed lines) configuration. The asymmetry is defined as distance separating the solute from the center of mass of the solvent shell. The structure is defined by the O – X^-/X^0 – O angles with X = Cl, Br, or I.

In addition to the plain coordination numbers, we investigated the structure and asymmetry of the first solvent shell (Figure 2). For Cl^-, Br^-, and I^-, the structuredness remains an intriguing question. Previous simulations were unable to provide a clear picture, i.e., some simulations[43,46,63,66] suggest a rather structured shell with a clear maximum of the O – $Cl^-/Br^-/I^-$ – O angle within 60 – 90 °, while other simulations[75,112], based on comparable theoretical methods, suggest a more unstructured shell. In addition, D'Angelo et al[112] concluded that EXAFS spectra calculated from an unstructured shell, derived by short QM simulations, are in better agreement with experimental signals than spectra calculated from a structured shell, derived by classical MD simulations. To determine the O – $Cl^-/Br^-/I^-$ – O angle in our AdBuff QM/MM simulations, we defined the shell as all water molecules with a hydrogen atom within the first hydrogen peak. Thereby, we obtained distributions for Cl^-, Br^-, and I^- with a clear maximum within 60 – 90 °, a tail extending up to 180 ° and a shoulder around 120 ° for Br^- and I^-, suggesting rather structured shells. To further confirm this assumption, we aligned

the oxygen atoms of the individual solvent shell configurations, which was possible with a low RMSD around 1 Å, supporting a suggestion by Raugei et al[46] that situations in which water molecules enter or leave the shell at different sites could be imaged as pseudorotations of the shell around the ion.

For the atom configuration, the AdBuff QM/MM simulations reveal broader O – Cl^0/Br^0/I^0 – O angle distributions with a less pronounced maximum around 90 °, suggesting rather unstructured shells. No comparisons from the literature are available for the atom case. The asymmetry of the first solvent shell was characterized before as the distance separating the solute from the center of mass of the shell. For Br^-, Raugei et al[46] determined an asymmetry of 1 – 4 Å, while D'Angelo et al[112] determined an asymmetry around 0.5 Å. Our AdBuff QM/MM simulations of Cl^-, Br^-, and I^- suggest a slightly increasing asymmetry with increasing ion size. For Br^- the asymmetry is within the range spanned by Raugei et al[46] and D'Angelo et al[112]. Compared to the solvent shell of the ions, the solvent shell of the atoms shows almost no asymmetry.

Overall, with the exception of the oxygen RDF minimum being too far out (and possibly too shallow), the AdBuff QM/MM simulations are in good agreement with previous investigations of halide ions and halogen atoms in water. This suggests that they provide a good basis for simulations of the systems' EXAFS spectra.

4 Simulation of EXAFS Spectra

For a direct comparison with experimental data[42], we have calculated EXAFS spectra as described in Section 2. Care needs to be taken with respect to the shift of EXAFS spectra along the energy or k-axis[116]. For this, we first convert the pure averaged EXAFS signal $\chi'(k')$ to energy space. The signal $\chi'(E')$ is then shifted by a certain value ΔE_0 (as specified below) in energy space and then transformed back to $\chi(k)$ in wavenumber (k) space. Multiplying by a

weighting factor k^3, we get the shifted signal $\chi(k)k^3$. We determine $\chi(k)k^3$ in the following for each of the three halides in both charge states.

The energy shift ΔE_0 of the EXAFS spectra accounts for the finite energy range in which the rise of the absorption signal at the absorption edge occurs[116]. The flank is never infinitely sharp and thus allows for a certain variation of the edge energy, which is assumed as arbitrarily sharp. This shift in energy is justified as long as its specific values remain within the uncertainty given by the finite width of the step at the absorption edge (see below for details).

In passing, we note that for the cases of the neutral atoms discussed below, no experimental reference data are available. We thus apply the same shift for the neutral atom data as that for the corresponding ion, which is further motivated by the fact that the inner orbitals are almost not affected by the presence of an outer electron or hole.

To obtain quantitative spatial information, we furthermore calculate the spatial Fourier transform of $\chi(k)k^3$. The results of this Fourier transform, together with the Fourier transform of the experimental data, are also shown below for the different halides. The Fourier transforms usually show a distinct maximum at a specific distance between the respective halide X and the oxygen atom of the water molecule, which we denote by R_{EXAFS}. In the following, we compare our EXAFS spectra calculated on the basis of the QM/MM configurations and FEFF8 to those obtained from experimental measurements and subsequent fittings in Ref.[42]. We also compare the energy shifts ΔE_0 obtained here and in Ref.[42]. Moreover, we directly compare the distances R_{sim} between O and the halide X obtained from the QM/MM as discussed in the previous section to the results obtained in Ref.[42] from the corresponding simulations. For convenience, we compile all values in Tab. 2.

Table 2: Distances between the halide X and the oxygen atom O of the water molecule as obtained from the MD simulations as maxima in the radial distribution functions (R_{sim}) as well as extracted from EXAFS spectra (R_{EXAFS}). For R_{sim}, we compare our results given in Tab. 1 with the simulated ones in Ref.[42]. For R_{EXAFS}, we analyze the EXAFS spectra calculated in Sec. 4.1 and compare the results with the experimental ones in Ref.[42]. In addition, we show the energy shifts ΔE_0 used for the EXAFS spectra as determined in Sec. 4.1 and compare these values with those of Ref.[42].

	Ref.	Cl^-	Br^-	I^-
R_{sim}(O−X) [Å]	this work	3.17	3.41	3.62
	[42]	3.15	3.28	3.50
R_{EXAFS} (O−X) [Å]	this work	2.55	2.6	2.7
	[42]	2.3	2.6	2.7
ΔE_0 [eV]	this work	1.52	9.41	8.02
	[42]	-11.047	0.0599	-0.4598

4.1 EXAFS spectra from QM/MM simulations

4.1.1 Solvated ions

In Fig. 3 (a), the averaged K-edge EXAFS for a hydrated Cl^- ion is shown as it follows from FEFF on the basis of the QM/MM MD configurations (blue solid line). The spectrum is shifted in k horizontally as described above. We use the energy shift of $\Delta E_0 = 1.52$ eV, which is consistent with the finite width of the energy range of about 5 eV in which the K-edge rises (see Fig. 7 in Ref.[42]).

We observe a decaying oscillatory pattern, indicating constructive and destructive interference of the generated photoelectron wave with its backscattered part. In addition, we show the experimental data of Ref.[42] for comparison. In general, we observe that the simulated EXAFS signal decays slightly faster than the experimental one, indicating faster decaying spatial coherence. Otherwise, we find a decent agreement between theory and experiment. In the Fourier transform of $\chi(k)k^3$, shown in Fig. 4 (a), we find a strong and broadened peak at 2.45 Å in

both the simulation and the experimental data. The small shoulder around 1 Å originates from the hydrogen atom, see the discussion below.

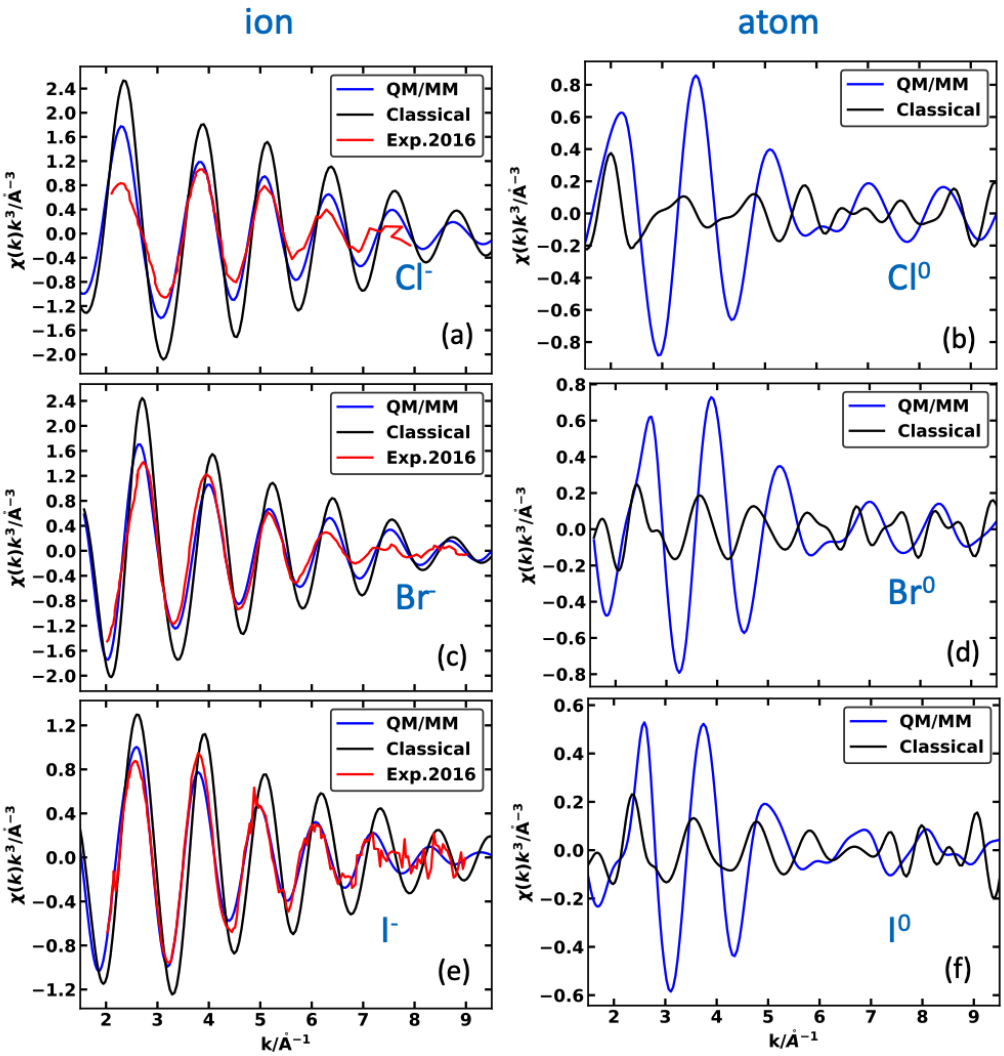

Figure 3: Left column: Averaged EXAFS spectrum $\chi(k)k^3$ for Cl^- (K-edge), Br^- (K-edge), and I^- (L1-edge) ions in water calculated via FEFF based on QM/MM (blue) and classical MD simulations (black), together with experimental EXAFS data (red) taken from Ref.[42]. Right column: The same for the corresponding atoms (without the comparison to experiment due to lack of data).

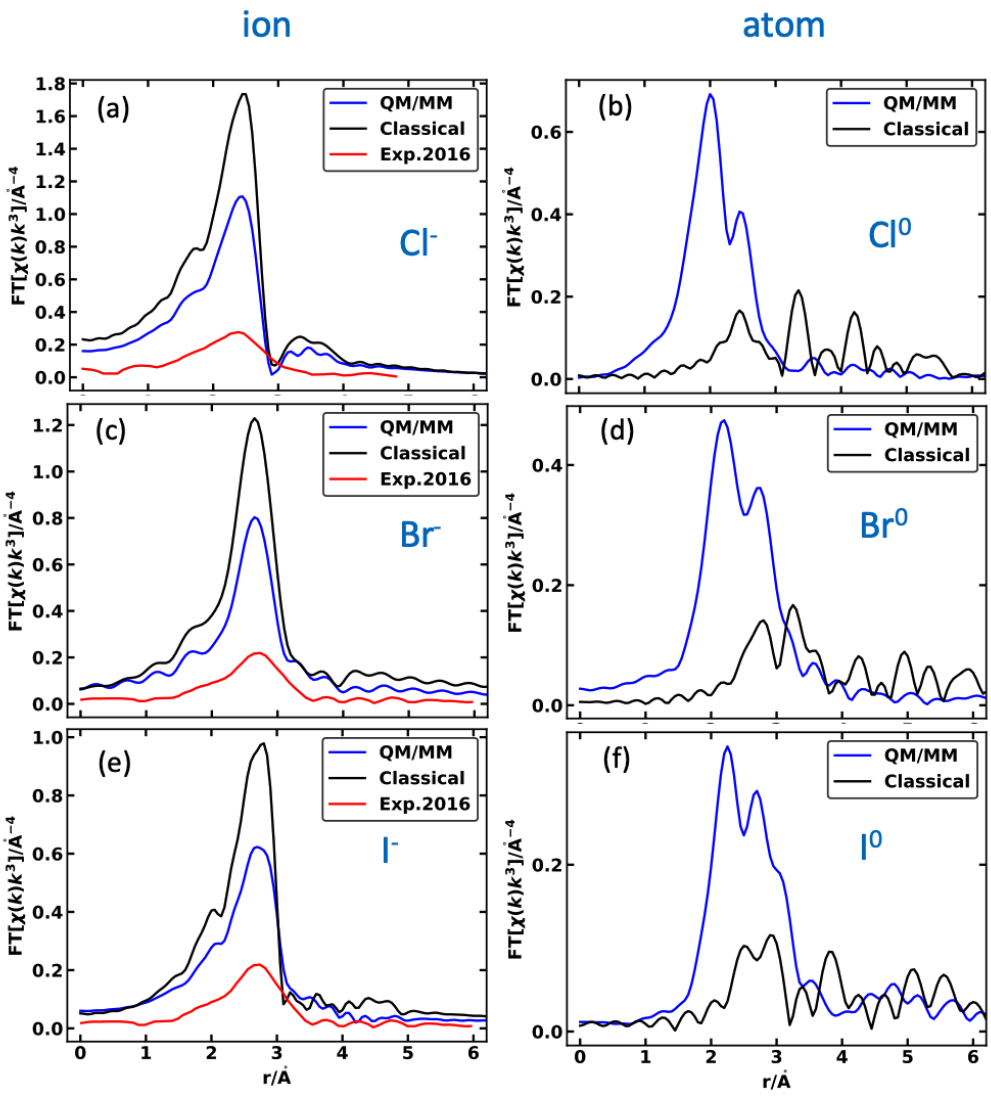

Figure 4: Fourier transforms of the QM/MM (blue) and measured (red) EXAFS spectra shown in Figure 3. Experimental data for the ions are taken from Ref.[42]. For the atoms, no such data were available.

In order to obtain spatial information about the individual atom species, we have calculated the EXAFS spectra and the corresponding Fourier transforms for configurations in which only all oxygen atoms and the solute atom, or all hydrogen atoms and the solute atom have been selected. The results are shown in Fig. S1 in the Supporting Information. The Fourier transforms are consistent with the hydrogen atoms pointing to the Cl^- solute, as the Cl−H distance (1.7 Å) is smaller than the Cl−O distance (2.55 Å). In addition, the backscattering from the oxygen

atoms is stronger than from the hydrogen atoms. From the spectrum of the complete water molecules, we observe that the main peak is closely associated to the peak of the oxygen atom, Fig. S1 (a)-(c), while the shoulder at smaller values of r can be traced back to the (weaker) peak of the hydrogen contribution shown in Fig. S1 (d).

In Fig. 3(c), the calculated averaged K-edge EXAFS spectrum for hydrated Br^- is shown, shifted by $\Delta E_0 = 9.41$ eV in energy and is compared to the experimental spectrum [42]. The energy shift is larger than for Cl^-, but it is consistent with the finite energy window of about 12 eV known from the experiment, see Fig. 5 in Ref. [42]. Again, a good agreement with the experiment is found, given that no phenomenological Debye-Waller factor has been used. This also holds for the the corresponding Fourier transformation shown in Fig. 4(c).

In Fig. S3 in the Supporting Information, the averaged K-edge EXAFS spectra for Br^- as solute is shown when only the hydrogen (a), only the oxygen (b) and the complete water molecule (c) is taken into account, along with the corresponding Fourier transforms in Fig. S3 (d) to (f). Also here, the hydrogen atoms point towards the Br^- since they are closer to the solute (Br−H distance 1.75 Å), compared to the negatively charged oxygen atom (Br−O distance 2.6 Å). The Fourier spectrum is composed of the dominating oxygen peak, while the hydrogen part generates the shoulder at smaller values of r.

Finally, Fig. 3 (e) shows the averaged L1-edge EXAFS spectrum of I^-, which includes a shift in energy by $\Delta E_0 = 8.02$ eV. The large value of ΔE_0 is still reasonable and within the finite energy window of the rise of the L1-edge signal, see Fig. 3 of Ref. [42]. The spectrum agrees well with the measured one taken from Ref. [42], and the same holds for the Fourier transformations shown in Fig. 4 (e).

Also in this case, we consider the different contributions of the atom species. In Fig. S5 of the Supporting Information, the averaged L1-edge EXAFS spectra for I^- and their Fourier transforms are shown, where the hydrogen and oxygen atoms have been activated separately. This leads to the same qualitative picture as for the chloride and bromide ions, with an I−H

distance of 1.9 Å and an I−O distance of 2.7 Å.

Overall, comparing the three halides, they show similar qualitative patterns in the EXAFS. Not surprisingly, the distances between the ions and their solvent shells increase as we go down the periodic table in the sequence $Cl^- \rightarrow Br^- \rightarrow I^-$, mirroring a corresponding increase in the positions of the RDF maxima (also compare Table 2.

4.1.2 Solvated neutral atoms

Next, we consider the neutral Cl^0 in water. Since no experimental data are available, we only show the theoretical curves in Fig. 3 (b) (QM/MM: blue line), with the same value of the energy shift as for the ion. We observe a beating pattern which is reflected in the two-peak structure in the Fourier transform in Fig. 4 (b). From the analysis of the separated contributions of oxygen and hydrogen atomsm shown in Fig. S2 in the Supporting Information, we find that two shells of water molecules exist. The inner shell has a radius of 2.0 Å, while the second shell appears at a radius of 2.45 Å.

Fig. 3 (d) shows the averaged EXAFS spectrum of Br^0 in water shifted in energy by the same amount as for Br^-. Fig. 4 (d) depicts the corresponding calculated Fourier transform. As for the neutral Cl^0 case, we also observe a beating pattern in the calculated EXAFS, together with a two-peak structure in the Fourier transform. This, again, indicates that two shells of water molecules exist for the neutral solutes. The first layer has a radius of 2.2 Å, while the second layer appears at 2.75 Å. The corresponding element-specific results are depicted in Fig. S4 in the Supporting Information, suggesting a similar qualitative picture as for Cl^0.

Finally, the averaged L1-edge EXAFS spectra of the neutral I^0 atom is shown in Fig. 3 (f), and its Fourier transform in Fig. 4 (f). Again, we have applied the same shift in energy as for the ion. Similar as above, we also observe a beating which goes along with two close-by peaks in the Fourier transform. Also here, two shells of water molecules are revealed from the EXAFS spectra. The first layer has a radius of 2.25 Å, while the second layer appears at 2.7

Å. The corresponding element specific spectra for I^0 are provided in Fig. S6 of the Supporting Information.

Overall, the atoms show similar qualitative EXAFS spectra for all three species, with (again, little surprisingly) the distance between atom and solvation shell increasing as we go to the heavier homologues. Compared to the ions, the EXAFS spectra have a beating pattern, resulting in a two-peak structure in the Fourier-transformed spectra, with the main peaks located at about half an Angstrøm smaller r values. These substantial differences suggest that EXAFS may be a suitable method for monitoring the dynamics following photoionization of aqueous halides.

4.1.3 Why are interatomic distances from MD simulations and from EXAFS data so different?

For all three cases considered, the X−H and X−O distances obtained from the EXAFS (both experimentally and theoretically) are much smaller than the distances obtained from the peaks in the calculated radial distribution function, as reported above. The reason for these differences is that the experimental EXAFS includes inherently a k-dependent shift of the scattering phase $\delta(k)$. This is an unavoidable feature of the method. The calculated radial distribution function does not have this feature, such that the obtained distances are not affected by a phase shift. In principle, the EXAFS signal could be corrected by the phase shift in order to match the results of the radial distribution function, which, however, requires introducing additional assumptions in the EXAFS.

4.2 EXAFS spectra from classical MD simulations

As shown in Sec. 3, QM/MM and classical MD simulations may lead to quite different radial distribution functions. From this and from the above comparison between experimental and

QM/MM EXAFS spectra, the question arises how much the differences in the underlying MD methodology actually affect the observables to be compared with the experiment in the case of EXAFS. To clarify this, we have also calculated the EXAFS spectra on the basis of molecular configurations obtained from purely classical molecular dynamics (MD) simulations for all three halides and and their neutral counterparts in water. As above, we show the averaged EXAFS spectra for the different cases multiplied by k^3 as is commonly shown, i.e., $\chi(k)k^3$.

4.2.1 Solvated anions

The simulated EXAFS spectra of the family of hydrated ions are shown in the left column of Figure 3 (black solid line), i.e., panels (a) for Cl^- , (c) for Br^-, and (e) for I^-. We depict the calculated EXAFS spectra coming from the classical MD simulations together with the corresponding EXAFS spectra obtained on the basis of QM/MM data (blue lines). We find that the oscillation period of EXAFS signal obtained from the classically calculated configurations matches that of the corresponding QM/MM data. Yet, the oscillation amplitudes are constantly larger for the classical case as compared to the QM/MM case, accordingly leading to stronger deviations from the experiment.

For completeness, the corresponding Fourier transforms of the EXAFS spectra to real space are also shown as black solid lines in Fig. 4, which also coincide with the results obtained with QM/MM MD configurations.

4.2.2 Solvated neutral atoms

The situation is different when we consider the EXAFS spectra for the neutral atoms obtained from classical MD configurations. The results are shown in the right column of Fig. 3 as black lines, i.e., panels (b) for Cl^0 , (d) for Br^0, and (f) for I^0. In all three cases, the spectra obtained with classical configurations are very different from the QM/MM data (shown in blue), both in terms of oscillating period and in absolute signal values, illustrating that for the neutral atoms,

a proper treatment of chemical bonding as provided by the QM part of QM/MM simulations are very important, much more so than for the ions. This holds also for the Fourier transforms, as shown as black solid lines in Fig. 4.

5 Conclusion and Outlook

We have studied the structure and dynamics of the solvation shells of aqueous halides and their atoms, as idealized models for charge centers in electron transfer reactions. The lack of solute nuclear degrees of freedom has allowed for a pure focus on the solvent. We have carried out molecular dynamics simulations and subsequently modeled EXAFS spectra based on the MD snapshots, without introducing any of the commonly used "fudge factors". From the analysis of these data, along with a comparison with the literature, we can draw the following conclusions:

For the ion case, our adaptive buffered QM/MM MD simulations agree quite well with their purely classical (force-field) counterparts. The main exception is the minimum in the QM/MM $X^- - O$ radial distribution functions, which is by about 1-1.5 Å further out (and much more shallow) than the classical one and than representative literature values obtained from various methods, including experimental neutron diffraction data. Only for I^- are there comparatively large QM/MM values to be found in the literature for this quantity. These differences could stem from the minimum being somewhere close to the radius of the QM area in the simulations, which may lead to discrepancies with other methods and also within the family of QM/MM approaches. For the peaks in the RDF, the QM/MM simulations match the neutron diffraction data a bit better than the classical ones.

Despite these differences, the EXAFS spectra obtained from superimposing simulated data for the MD snapshots agree well with the experiment for both QM/MM and classical simulations. In particular, the oscillation period is the same for both approaches. Yet, the oscillation amplitudes show some deviations, with the QM/MM data matching better the experimental data

sets. On the one hand, this suggests that as long as the MD simulations give a qualitatively good description of the RDFs, they will be able to predict the oscillation period of the EXAFS spectra well. On the other hand, this implies that to judge the reliability of theoretical simulation methods or to elucidate fine details of the atomistic dynamics of the solvent based on EXAFS spectra, the amplitude and not only the oscillatory period need to be considered.

In contrast, the radial distribution functions for the atomic case look vastly different for QM/MM and purely classical MD simulations (as one would expect given the inability of a standard force field to describe the bonding of open-shell species to their closed-shell surroundings). In this case, the simulated EXAFS spectra differ clearly from each other, both with respect to amplitude and oscillatory period, suggesting that EXAFS is sensitive to such large qualitative differences in the atomistic structure and dynamics.

Even though for the atoms, a comparison with the experiment is not possible due to lack of data, the general ability of QM/MM methods to describe radical–water bonding, together with the good agreement of this method with the ions' experimental EXAFS spectra, suggests that the QM/MM-based EXAFS spectra are reliable also for the solvated-atom case. Thus, these simulations can likely provide a basis for further studies towards nonequilibrium solvent dynamics following photoionization (ideally taking into account nonadiabatic effects[117–121]), which should be favored by the clearly distinctive EXAFS spectra for ions and atoms found in our simulations. Such studies may later be extended towards electron transfer processes in more complex systems, with the eventual goal of including biological activity in physiological media.

Acknowledgement

This work is supported by the Cluster of Excellence "Advanced Imaging of Matter" of the Deutsche Forschungsgemeinschaft (DFG) — EXC 2056 — project ID 390715994. The authors

thank the High-Performance Computing Center at Universität Hamburg for computational resources. We thank Mariana Rossi, MPSD Hamburg, for helpful discussions.

Supporting Information Available

In the Supporting Information, we show the calculated element-specific EXAFS spectra when only the respective element sub-class of the water molecule is included.

References

(1) Berg, J. M.; Stryer, L.; Tymoczko, J. L.; Gatto, G. *Biochemistry*, 9th ed.; Freeman: New York, 2019.

(2) Dempsey, J. L.; Winkler, J. R.; Gray, H. B. Proton-Coupled Electron Flow in Protein Redox Machines. *Chem. Rev.* **2010**, *110*, 7024–7039.

(3) Seefeldt, L. C.; Hoffman, B. M.; Dean, D. R. Electron transfer in nitrogenase catalysis. *Curr. Opin. Chem. Biol.* **2012**, *16*, 19–25.

(4) Studer, A.; Curran, D. P. Organocatalysis and C-H Activation Meet Radical- and Electron-Transfer Reactions. *Angew. Chem. Int. Ed.* **2011**, *50*, 5018–5022.

(5) Ghosh, I.; Shaikh, R. S.; König, B. Sensitization-Initiated Electron Transfer for Photoredox Catalysis. *Angew. Chem. Int. Ed.* **2017**, *56*, 8544–8549.

(6) Kärkäs, M. D.; Johnston, E. V.; Verho, O.; Åkermark, B. Artificial Photosynthesis: From Nanosecond Electron Transfer to Catalytic Water Oxidation. *Acc. Chem. Res.* **2014**, *47*, 100–111.

(7) Mora, S. J.; Odella, E.; Moore, G. F.; Gust, D.; Moore, T. A.; Moore, A. L. Proton-Coupled Electron Transfer in Artificial Photosynthetic Systems. *Acc. Chem. Res.* **2018**, *51*, 445–453.

(8) Maroncelli, M.; MacInnis, J.; Fleming, G. R. Polar Solvent Dynamics and Electron-Transfer Reactions. *Science* **1989**, *243*, 1674–1681.

(9) Schenter, G. K.; Garrett, B. C.; Truhlar, D. G. The Role of Collective Solvent Coordinates and Nonequilibrium Solvation in Charge-Transfer Reactions. *The Journal of Physical Chemistry B* **2001**, *105*, 9672–9685.

(10) Bjorgaard, J. A.; Velizhanin, K. A.; Tretiak, S. Nonequilibrium solvent effects in Born-Oppenheimer molecular dynamics for ground and excited electronic states. *J. Chem. Phys.* **2016**, *144*, 154104.

(11) Li, X.-Y. An overview of continuum models for nonequilibrium solvation: Popular theories and new challenge. *International Journal of Quantum Chemistry* **2015**, *115*, 700–721.

(12) Lu, Y.; Kundu, M.; Zhong, D. Effects of nonequilibrium fluctuations on ultrafast short-range electron transfer dynamics. *Nat. Commun.* **2020**, *11*, 2822.

(13) Yang, J.; Zhang, Y.; Lu, Y.; Wang, L.; Lu, F.; Zhong, D. Ultrafast Dynamics of Nonequilibrium Short-Range Electron Transfer in Semiquinone Flavodoxin. *J. Chem. Phys. Lett.* **2022**, *13*, 3202–3208.

(14) Wörner, H. J. et al. Charge migration and charge transfer in molecular systems. *Struct. Dyn.* **2017**, *4*, 061508.

(15) Hage, K. E.; Brickel, S.; Hermelin, S.; Gaulier, G.; Schmidt, C.; Bonacina, L.; van Keulen, S. C.; Bhattacharyya, S.; Chergui, M.; Hamm, P.; Rothlisberger, U.; Wolf, J.-P.; Meuwly, M. Implications of short time scale dynamics on long time processes. *Struct. Dyn.* **2017**, *4*, 061507.

(16) Chergui, M. Ultrafast photoinduced energy and charge transfer. *Faraday Discuss.* **2019**, *216*, 9–37.

(17) Chergui, M. Time-resolved X-ray spectroscopies of chemical systems: New perspectives. *Struct. Dyn.* **2016**, *3*, 031001.

(18) Dell'Angela, M.; Parmigiani, F.; Malvestuto, M. Time resolved X-ray absorption spectroscopy in condensed matter: A road map to the future. *J. Electron Spectrosc.* **2015**, *200*, 22–30.

(19) Bartlett, S. A.; Hamilton, M. L.; Evans, J. Dynamic structure elucidation of chemical reactivity by laser pulses and X-ray probes. *Dalton T.* **2015**, *44*, 6313–6319.

(20) Canton, S. E. et al. Visualizing the non-equilibrium dynamics of photoinduced intramolecular electron transfer with femtosecond X-ray pulses. *Nat. Commun.* **2015**, *6*.

(21) Rondi, A.; Rodriguez, Y.; Feurer, T.; Cannizzo, A. Solvation-Driven Charge Transfer and Localization in Metal Complexes. *Acc. Chem. Res.* **2015**, *48*, 1432–1440.

(22) Biasin, E. et al. Direct observation of coherent femtosecond solvent reorganization coupled to intramolecular electron transfer. *Nat. Chem.* **2021**, *13*, 343–349.

(23) Biasin, E. et al. Author Correction: Direct observation of coherent femtosecond solvent reorganization coupled to intramolecular electron transfer. *Nat. Chem.* **2021**, *14*, 474–474.

(24) Monroe, J.; Barry, M.; DeStefano, A.; Gokturk, P. A.; Jiao, S.; Robinson-Brown, D.; Webber, T.; Crumlin, E. J.; Han, S.; Shell, M. S. Water Structure and Properties at Hydrophilic and Hydrophobic Surfaces. *Annu. Rev. Chem. Biomol.* **2020**, *11*, 523–557.

(25) Elles, C. G.; Shkrob, I. A.; Crowell, R. A.; Arms, D. A.; Landahl, E. C. Transient x-ray absorption spectroscopy of hydrated halogen atom. *J. Chem. Phys.* **2008**, *128*, 061102.

(26) Kloepfer, J. A.; Vilchiz, V. H.; Lenchenkov, V. A.; Bradforth, S. E. Femtosecond dynamics of photodetachment of the iodide anion in solution: resonant excitation into the charge-transfer-to-solvent state. *Chemical Physics Letters* **1998**, *298*, 120–128.

(27) Vilchiz, V. H.; Kloepfer, J. A.; Germaine, A. C.; Lenchenkov, V. A.; Bradforth, S. E. Map for the Relaxation Dynamics of Hot Photoelectrons Injected into Liquid Water via Anion Threshold Photodetachment and above Threshold Solvent Ionization. *The Journal of Physical Chemistry A* **2001**, *105*, 1711–1723.

(28) Bressler, C.; Saes, M.; Chergui, M.; Grolimund, D.; Abela, R.; Pattison, P. Towards structural dynamics in condensed chemical systems exploiting ultrafast time-resolved x-ray absorption spectroscopy. *The Journal of Chemical Physics* **2002**, *116*, 2955–2966.

(29) Chen, X.; Bradforth, S. E. The Ultrafast Dynamics of Photodetachment. *Annu. Rev. Phys. Chem.* **2008**, *59*, 203–231.

(30) Kloepfer, J. A.; Vilchiz, V. H.; Lenchenkov, V. A.; Germaine, A. C.; Bradforth, S. E. The ejection distribution of solvated electrons generated by the one-photon photodetachment of aqueous I- and two-photon ionization of the solvent. *J. Chem. Phys.* **2000**, *113*, 6288–6307.

(31) Kloepfer, J. A.; Vilchiz, V. H.; Lenchenkov, V. A.; Chen, X.; Bradforth, S. E. Time-resolved scavenging and recombination dynamics from I:e− caged pairs. *The Journal of Chemical Physics* **2002**, *117*.

(32) Sauer, M. C.; Crowell, R. A.; Shkrob, I. A. Electron Photodetachment from Aqueous Anions. 1. Quantum Yields for Generation of Hydrated Electron by 193 and 248 nm Laser Photoexcitation of Miscellaneous Inorganic Anions. *The Journal of Physical Chemistry A* **2004**, *108*, 5490–5502.

(33) Sauer, M. C.; Shkrob, I. A.; Lian, R.; Crowell, R. A.; Bartels, D. M.; Chen, X.; Suffern, D.; Bradforth, S. E. Electron Photodetachment from Aqueous Anions. 2. Ionic Strength

Effect on Geminate Recombination Dynamics and Quantum Yield for Hydrated Electron. *The Journal of Physical Chemistry A* **2004**, *108*, 10414–10425.

(34) Iglev, H.; Trifonov, A.; Thaller, A.; Buchvarov, I.; Fiebig, T.; Laubereau, A. Photoionization dynamics of an aqueous iodide solution: the temperature dependence. *Chemical Physics Letters* **2005**, *403*, 198–204.

(35) Lian, R.; Oulianov, D. A.; Crowell, R. A.; Shkrob, I. A.; Chen, X.; Bradforth, S. E. Electron Photodetachment from Aqueous Anions. 3. Dynamics of Geminate Pairs Derived from Photoexcitation of Mono- vs Polyatomic Anions. *The Journal of Physical Chemistry A* **2006**, *110*, 9071–9078, PMID: 16854017.

(36) Iglev, H.; Laubereau, A. Electron detachment and recombination in aqueous solutions studied with 2- and 3-pulse femtosecond spectroscopy. Laser Applications in Life Sciences. 2010; pp 201 – 209.

(37) Messina, F.; Bräm, O.; Cannizzo, A.; Chergui, M. Real-time observation of the charge transfer to solvent dynamics. *Nat. Commun.* **2013**, *4*.

(38) Pham, V.-T.; Penfold, T. J.; van der Veen, R. M.; Lima, F.; Nahhas, A. E.; Johnson, S. L.; Beaud, P.; Abela, R.; Bressler, C.; Tavernelli, I.; Milne, C. J.; Chergui, M. Probing the Transition from Hydrophilic to Hydrophobic Solvation with Atomic Scale Resolution. *J. Am. Chem. Soc.* **2011**, *133*, 12740–12748.

(39) Pham, V.-T.; Gawelda, W.; Zaushitsyn, Y.; Kaiser, M.; Grolimund, D.; Johnson, S. L.; Abela, R.; Bressler, C.; Chergui, M. Observation of the Solvent Shell Reorganization around Photoexcited Atomic Solutes by Picosecond X-ray Absorption Spectroscopy. *J. Am. Chem. Soc.* **2007**, *129*, 1530–1531.

(40) Sessa, F.; D'Angelo, P.; Guidoni, L.; Migliorati, V. Hidden Hydration Structure of Halide Ions: an Insight into the Importance of Lone Pairs. *The Journal of Physical Chemistry B* **2015**, *119*, 15729–15737, PMID: 26629711.

(41) D'Angelo, P.; Migliorati, V.; Guidoni, L. Hydration properties of the bromide aqua ion: the interplay of first principle and classical molecular dynamics, and X-ray absorption spectroscopy. *Inorganic chemistry* **2010**, *49*, 4224–4231.

(42) Antalek, M.; Pace, E.; Hedman, B.; Hodgson, K. O.; Chillemi, G.; Benfatto, M.; Sarangi, R.; Frank, P. Solvation structure of the halides from x-ray absorption spectroscopy. *The Journal of chemical physics* **2016**, *145*, 044318.

(43) Tongraar, A.; Michael Rode, B. The hydration structures of F− and Cl− investigated by ab initio QM/MM molecular dynamics simulations. *Phys. Chem. Chem. Phys.* **2003**, *5*, 357–362.

(44) Tongraar, A.; T-Thienprasert, J.; Rujirawat, S.; Limpijumnong, S. Structure of the hydrated Ca2+ and Cl−: Combined X-ray absorption measurements and QM/MM MD simulations study. *Phys. Chem. Chem. Phys.* **2010**, *12*, 10876–10887.

(45) Pham, V.; Tavernelli, I.; Milne, C.; van der Veen, R.; D'Angelo, P.; Bressler, C.; Chergui, M. The solvent shell structure of aqueous iodide: X-ray absorption spectroscopy and classical, hybrid QM/MM and full quantum molecular dynamics simulations. *Chem. Phys.* **2010**, *371*, 24–29.

(46) Raugei, S.; Klein, M. L. An ab initio study of water molecules in the bromide ion solvation shell. *J. Chem. Phys.* **2002**, *116*, 196–202.

(47) Impey, R. W.; Madden, P. A.; McDonald, I. R. Hydration and mobility of ions in solution. *The Journal of Physical Chemistry* **1983**, *87*, 5071–5083.

(48) Tóth, G. Ab initio pair potential parameter set for the interaction of a rigid and a flexible water model and the complete series of the halides and alkali cations. *The Journal of Chemical Physics* **1996**, *105*, 5518–5524.

(49) Gladich, I.; Shepson, P.; Szleifer, I.; Carignano, M. Halide and sodium ion parameters for

modeling aqueous solutions in TIP5P-Ew water. *Chemical Physics Letters* **2010**, *489*, 113–117.

(50) Degrève, L.; de Pauli, V. M.; Duarte, M. A. Simulation study of the role and structure of monatomic ions multiple hydration shells. *The Journal of Chemical Physics* **1997**, *106*, 655–665.

(51) Symons, M. C. R.; Neilson, G. W.; Mason, P. E.; Ramos, S.; Sullivan, D. Neutron and X-ray scattering studies of hydration in aqueous solutions. *Philosophical Transactions of the Royal Society of London. Series A: Mathematical, Physical and Engineering Sciences* **2001**, *359*, 1575–1591.

(52) Soper, A. K.; Weckström, K. Ion solvation and water structure in potassium halide aqueous solutions. *Biophysical Chemistry* **2006**, *124*, 180–191.

(53) Merkling, P. J.; Ayala, R.; Martinez, J. M.; Pappalardo, R. R.; Sánchez Marcos, E. Interplay of computer simulations and x-ray absorption spectra in the study of the bromide hydration structure. *The Journal of Chemical Physics* **2003**, *119*, 6647–6654.

(54) D'Angelo, P.; Di Nola, A.; Filipponi, A.; Pavel, N. V.; Roccatano, D. An extended x-ray absorption fine structure study of aqueous solutions by employing molecular dynamics simulations. *The Journal of Chemical Physics* **1994**, *100*, 985–994.

(55) Smirnov, P. Structural parameters of the nearest surrounding of halide ions in the aqueous electrolyte solutions. *Russ J Gen Chem* **2013**, *83*, 1469–1481.

(56) Baer, M. D.; Fulton, J. L.; Balasubramanian, M.; Schenter, G. K.; Mundy, C. J. Persistent Ion Pairing in Aqueous Hydrochloric Acid. *The Journal of Physical Chemistry B* **2014**, *118*, 7211–7220, PMID: 24837190.

(57) Filipponi, A.; De Panfilis, S.; Oliva, C.; Ricci, M. A.; D'Angelo, P.; Bowron, D. T. Ion hydration under pressure. *Physical review letters* **2003**, *91*, 165505.

(58) Fulton, J. L.; Balasubramanian, M. Structure of Hydronium (H3O+)/Chloride (Cl−) Contact Ion Pairs in Aqueous Hydrochloric Acid Solution: A Zundel-like Local Configuration. *Journal of the American Chemical Society* **2010**, *132*, 12597–12604, PMID: 20731390.

(59) Powell, D. H.; Neilson, G. W.; Enderby, J. E. The structure of Cl^-in aqueous solution: an experimental determination of gClH(r) and gClO(r). *Journal of Physics: Condensed Matter* **1993**, *5*, 5723–5730.

(60) Tanida, H.; Sakane, H.; Watanabe, I. Solvation structures for bromide ion in various solvents by extended X-ray absorption fine structure. *J. Chem. Soc., Dalton Trans.* **1994**, 2321–2326.

(61) Smith, J. D.; Saykally, R. J.; Geissler, P. L. The Effects of Dissolved Halide Anions on Hydrogen Bonding in Liquid Water. *Journal of the American Chemical Society* **2007**, *129*, 13847–13856, PMID: 17958418.

(62) Humphrey, W.; Dalke, A.; Schulten, K. VMD – Visual Molecular Dynamics. *Journal of Molecular Graphics* **1996**, *14*, 33–38.

(63) DelloStritto, M.; Xu, J.; Wu, X.; Klein, M. L. Aqueous solvation of the chloride ion revisited with density functional theory: impact of correlation and exchange approximations. *Phys. Chem. Chem. Phys.* **2020**, *22*, 10666–10675.

(64) Tuñón, I.; Martins-Costa, M. T.; Millot, C.; Ruiz-López, M. F. Coupled density functional/molecular mechanics Monte Carlo simulations of ions in water. The bromide ion. *Chemical Physics Letters* **1995**, *241*, 450–456.

(65) Lev, B.; Roux, B.; Noskov, S. Y. Relative Free Energies for Hydration of Monovalent Ions from QM and QM/MM Simulations. *Journal of Chemical Theory and Computation* **2013**, *9*, 4165–4175.

(66) Heuft, J. M.; Meijer, E. J. Density functional theory based molecular-dynamics study of aqueous chloride solvation. *The Journal of Chemical Physics* **2003**, *119*, 11788–11791.

(67) Wick, C. D.; Xantheas, S. S. Computational Investigation of the First Solvation Shell Structure of Interfacial and Bulk Aqueous Chloride and Iodide Ions. *The Journal of Physical Chemistry B* **2009**, *113*, 4141–4146, PMID: 19014185.

(68) Bounds, D. A molecular dynamics study of the structure of water around the ions Li+, Na+, K+, Ca++, Ni++ and Cl-. *Molecular Physics* **1985**, *54*, 1335–1355.

(69) Koneshan, S.; Rasaiah, J. C.; Lynden-Bell, R. M.; Lee, S. H. Solvent Structure, Dynamics, and Ion Mobility in Aqueous Solutions at 25 °C. *The Journal of Physical Chemistry B* **1998**, *102*, 4193–4204.

(70) Probst, M. M.; Radnai, T.; Heinzinger, K.; Bopp, P.; Rode, B. M. Molecular dynamics and x-ray investigation of an aqueous calcium chloride solution. *The Journal of Physical Chemistry* **1985**, *89*, 753–759.

(71) Bankura, A.; Santra, B.; Jr., R. A. D.; Swartz, C. W.; Klein, M. L.; Wu, X. A systematic study of chloride ion solvation in water using van der Waals inclusive hybrid density functional theory. *Molecular Physics* **2015**, *113*, 2842–2854.

(72) Bruni, F.; Imberti, S.; Mancinelli, R.; Ricci, M. A. Aqueous solutions of divalent chlorides: Ions hydration shell and water structure. *The Journal of Chemical Physics* **2012**, *136*, 064520.

(73) Albright, J. N. X-Ray Diffraction Studies of Aqueous Alkaline-Earth Chloride Solutions. *The Journal of Chemical Physics* **1972**, *56*, 3783–3786.

(74) Brady, G. W. Structure in Ionic Solutions. IV. *The Journal of Chemical Physics* **1960**, *33*, 1079–1082.

(75) Heuft, J. M.; Meijer, E. J. Density functional theory based molecular-dynamics study of aqueous iodide solvation. *The Journal of Chemical Physics* **2005**, *123*, 094506.

(76) Penfold, T.; Tavernelli, I.; Doemer, M.; Abela, R.; Röthlisberger, U.; Chergui, M. Solvent rearrangements during the transition from hydrophilic to hydrophobic solvation. *Chem. Phys.* **2013**, *410*, 25–30.

(77) Dang, L. X.; Garrett, B. C. Photoelectron spectra of the hydrated iodine anion from molecular dynamics simulations. *The Journal of Chemical Physics* **1993**, *99*, 2972–2977.

(78) Karmakar, A.; Chandra, A. Water in Hydration Shell of an Iodide Ion: Structure and Dynamics of Solute-Water Hydrogen Bonds and Vibrational Spectral Diffusion from First-Principles Simulations. *The Journal of Physical Chemistry B* **2015**, *119*, 8561–8572, PMID: 26125325.

(79) Ayala, R.; Martinez, J. M.; Pappalardo, R. R.; Sánchez Marcos, E. On the halide hydration study: Development of first-principles halide ion-water interaction potential based on a polarizable model. *The Journal of Chemical Physics* **2003**, *119*, 9538–9548.

(80) Roeselová, M.; Kaldor, U.; Jungwirth, P. Ultrafast Dynamics of Chlorine−Water and Bromine−Water Radical Complexes Following Electron Photodetachment in Their Anionic Precursors. *The Journal of Physical Chemistry A* **2000**, *104*, 6523–6531.

(81) Migliorati, V.; Sessa, F.; Aquilanti, G.; D'Angelo, P. Unraveling halide hydration: A high dilution approach. *The Journal of Chemical Physics* **2014**, *141*, 044509.

(82) Caruso, A.; Paesani, F. Data-driven many-body models enable a quantitative description of chloride hydration from clusters to bulk. *J. Chem. Phys.* **2021**, *155*, 064502.

(83) Caruso, A.; Zhu, X.; Fulton, J. L.; Paesani, F. Accurate Modeling of Bromide and Iodide Hydration with Data-Driven Many-Body Potentials. *J. Phys. Chem. B* **2022**, *126*, 8266–8278.

(84) Heisler, I. A.; Meech, S. R. Low-Frequency Modes of Aqueous Alkali Halide Solutions: Glimpsing the Hydrogen Bonding Vibration. *Science* **2010**, *327*, 857–860.

(85) Heisler, I. A.; Mazur, K.; Meech, S. R. Low-Frequency Modes of Aqueous Alkali Halide Solutions: An Ultrafast Optical Kerr Effect Study. *J. Phys. Chem. B* **2011**, *115*, 1863–1873.

(86) Ohtaki, H.; Radnai, T. Structure and dynamics of hydrated ions. *Chemical Reviews* **1993**, *93*, 1157–1204.

(87) Krishnan, V.; Feth, M. P.; Wendel, E.; Chen, Y.; Hanack, M.; Bertagnolli, H. EXAFS Spectroscopy – Fundamentals, Measurement Techniques, Data Evaluation and Applications in the Field of Phthalocyanines. *Zeitschrift für Physikalische Chemie* **2004**, *218*, 1–16.

(88) Rehr, J. J.; Albers, R. C. Theoretical approaches to x-ray absorption fine structure. *Rev. Mod. Phys.* **2000**, *72*, 621–654.

(89) Atkins, A. J.; Bauer, M.; Jacob, C. R. The chemical sensitivity of X-ray spectroscopy: high energy resolution XANES versus X-ray emission spectroscopy of substituted ferrocenes. *Phys. Chem. Chem. Phys.* **2013**, *15*, 8095.

(90) Rudolph, J.; Jacob, C. R. Revisiting the Dependence of Cu K-Edge X-ray Absorption Spectra on Oxidation State and Coordination Environment. *Inorg. Chem.* **2018**, *57*, 10591–10607.

(91) Ferlat, G.; Soetens, J.-C.; Miguel, A. S.; Bopp, P. A. Combining extended x-ray absorption fine structure with numerical simulations for disordered systems. *Journal of Physics: Condensed Matter* **2005**, *17*, S145–S157.

(92) Cappa, C. D.; Smith, J. D.; Wilson, K. R.; Messer, B. M.; Gilles, M. K.; Cohen, R. C.; Saykally, R. J. Effects of Alkali Metal Halide Salts on the Hydrogen Bond Network

of Liquid Water. *The Journal of Physical Chemistry B* **2005**, *109*, 7046–7052, PMID: 16851801.

(93) Heuft, J. M.; Meijer, E. J. Density functional theory based molecular-dynamics study of aqueous chloride solvation. *The Journal of Chemical Physics* **2003**, *119*, 11788–11791.

(94) Wallen, S. L.; Palmer, B. J.; Pfund, D. M.; Fulton, J. L.; Newville, M.; Ma, Y.; Stern, E. A. Hydration of Bromide Ion in Supercritical Water: An X-ray Absorption Fine Structure and Molecular Dynamics Study. *The Journal of Physical Chemistry A* **1997**, *101*, 9632–9640.

(95) Kühne, T. D. et al. CP2K: An electronic structure and molecular dynamics software package - Quickstep: Efficient and accurate electronic structure calculations. *The Journal of Chemical Physics* **2020**, *152*, 194103.

(96) Jones, A.; Leimkuhler, B. Adaptive stochastic methods for sampling driven molecular systems. *The Journal of Chemical Physics* **2011**, *135*, 084125.

(97) Swope, W. C.; Andersen, H. C.; Berens, P. H.; Wilson, K. R. A computer simulation method for the calculation of equilibrium constants for the formation of physical clusters of molecules: Application to small water clusters. *The Journal of Chemical Physics* **1982**, *76*, 637–649.

(98) Becke, A. D. Density-functional exchange-energy approximation with correct asymptotic behavior. *Phys. Rev. A* **1988**, *38*, 3098–3100.

(99) Lee, C.; Yang, W.; Parr, R. G. Development of the Colle-Salvetti correlation-energy formula into a functional of the electron density. *Phys. Rev. B* **1988**, *37*, 785–789.

(100) Grimme, S.; Antony, J.; Ehrlich, S.; Krieg, H. A consistent and accurate ab initio parametrization of density functional dispersion correction (DFT-D) for the 94 elements H-Pu. *The Journal of Chemical Physics* **2010**, *132*, 154104.

(101) VandeVondele, J.; Hutter, J. Gaussian basis sets for accurate calculations on molecular systems in gas and condensed phases. *The Journal of Chemical Physics* **2007**, *127*, 114105.

(102) Goedecker, S.; Teter, M.; Hutter, J. Separable dual-space Gaussian pseudopotentials. *Phys. Rev. B* **1996**, *54*, 1703–1710.

(103) Hartwigsen, C.; Goedecker, S.; Hutter, J. Relativistic separable dual-space Gaussian pseudopotentials from H to Rn. *Phys. Rev. B* **1998**, *58*, 3641–3662.

(104) Krack, M. Pseudopotentials for H to Kr optimized for gradient-corrected exchange-correlation functionals. *Theor. Chem. Acc.* **2005**, *114*, 145–152.

(105) MacKerell, A. D. et al. All-Atom Empirical Potential for Molecular Modeling and Dynamics Studies of Proteins. *The Journal of Physical Chemistry B* **1998**, *102*, 3586–3616.

(106) Brooks, B. R. et al. CHARMM: The Biomolecular simulation Program. *J. Comp. Chem.* **2009**, *30*, 1545–1615.

(107) Mones, L.; Jones, A.; Götz, A. W.; Laino, T.; Walker, R. C.; Leimkuhler, B.; Csányi, G.; Bernstein, N. The adaptive buffered force QM/MM method in the CP2K and AMBER software packages. *Journal of Computational Chemistry* **2015**, *36*, 633–648.

(108) Martínez, L.; Andrade, R.; Birgin, E. G.; Martínez, J. M. PACKMOL: A package for building initial configurations for molecular dynamics simulations. *Journal of Computational Chemistry* **2009**, *30*, 2157–2164.

(109) Ankudinov, A.; Ravel, B.; Rehr, J.; Conradson, S. Real Space Multiple Scattering Calculation of XANES. *Phys. Rev. B* **1998**, *58*, 7565.

(110) Galamba, N. Mapping Structural Perturbations of Water in Ionic Solutions. *The Journal of Physical Chemistry B* **2012**, *116*, 5242–5250, PMID: 22480309.

(111) Zhou, J.; Lu, X.; Wang, Y.; Shi, J. Molecular dynamics study on ionic hydration. *Fluid Phase Equilibria* **2002**, *194-197*, 257–270, Proceedings of the Ninth International Conference on Properties and Phase Equilibria for Product and Process Design.

(112) D'Angelo, P.; Migliorati, V.; Guidoni, L. Hydration Properties of the Bromide Aqua Ion: the Interplay of First Principle and Classical Molecular Dynamics, and X-ray Absorption Spectroscopy. *Inorg. Chem.* **2010**, *49*, 4224–4231.

(113) Tongraar, A.; Hannongbua, S.; Rode, B. M. QM/MM MD Simulations of Iodide Ion (I−) in Aqueous Solution: A Delicate Balance between Ion−Water and Water−Water H-Bond Interactions. *The Journal of Physical Chemistry A* **2010**, *114*, 4334–4339.

(114) Hofer, T. S.; Tran, H. T.; Schwenk, C. F.; Rode, B. M. Characterization of dynamics and reactivities of solvated ions by ab initio simulations. *Journal of Computational Chemistry* **2004**, *25*, 211–217.

(115) Herdman, G.; Neilson, G. Neutron scattering studies of aqua-ions. *Journal of Molecular Liquids* **1990**, *46*, 165–179.

(116) Kelly, S. D.; Ravel, B. EXAFS energy shift and structural parameters. AIP Conference Proceedings. 2007; pp 132–134.

(117) Zederkof, D. B.; Møller, K. B.; Nielsen, M. M.; Haldrup, K.; González, L.; Mai, S. Resolving Femtosecond Solvent Reorganization Dynamics in an Iron Complex by Nonadiabatic Dynamics Simulations. *J. Am. Chem. Soc.* **2022**, *144*, 12861–12873.

(118) Avagliano, D.; Bonfanti, M.; Garavelli, M.; González, L. QM/MM Nonadiabatic Dynamics: the SHARC/COBRAMM Approach. *J. Chem. Theory Comput.* **2021**, *17*, 4639–4647.

(119) Song, H.; Fischer, S. A.; Zhang, Y.; Cramer, C. J.; Mukamel, S.; Govind, N.; Tretiak, S. First Principles Nonadiabatic Excited-State Molecular Dynamics in NWChem. *J. Chem. Theory Comput.* **2020**, *16*, 6418–6427.

(120) Schwerdtfeger, C. A.; Soudackov, A. V.; Hammes-Schiffer, S. Nonadiabatic dynamics of electron transfer in solution: Explicit and implicit solvent treatments that include multiple relaxation time scales. *J. Chem. Phys.* **2014**, *140*, 034113.

(121) Jain, A.; Alguire, E.; Subotnik, J. E. An Efficient, Augmented Surface Hopping Algorithm That Includes Decoherence for Use in Large-Scale Simulations. *J. Chem. Theory Comput.* **2016**, *12*, 5256–5268.

Graphical TOC Entry